Multiple Optical Elastography Techniques Reveal the Regulation of Corneal Stiffness by Collagen XII

Achuth Nair,[1] Yogeshwari S. Ambekar,[1] Christian Zevallos-Delgado,[1] Taye Mekonnen,[1] Mei Sun,[2] Fernando Zvietcovich,[3] Manmohan Singh,[1] Salavat Aglyamov,[4] Manuel Koch,[5] Giuliano Scarcelli,[6] Edgar M. Espana,[2,7] and Kirill V. Larin[1,8]

[1]Department of Biomedical Engineering, University of Houston, Houston, TX, United States
[2]Cornea and External Disease, Department of Ophthalmology, Morsani College of Medicine, University of South Florida, Tampa, Florida, United States
[3]Department of Engineering, Pontificia Universidad Catolica del Peru, San Miguel, Lima, Peru
[4]Department of Mechanical Engineering, University of Houston, Houston, TX, United States
[5]Institute for Dental Research and Oral Musculoskeletal Biology, Center for Molecular Medicine Cologne, and Center for Biochemistry, Medical Faculty, University of Cologne, Cologne, Germany
[6]Fischell Department of Bioengineering, University of Maryland, College Park, MD, United States
[7]Department of Molecular Pharmacology & Physiology, Morsani College of Medicine, University of South Florida, Tampa, Florida, United States
[8]Department of Molecular Physiology and Biophysics, Baylor College of Medicine, Houston, Texas, United States

Correspondence: Edgar M. Espana, 1330 USF Laurel Dr, Fourth Floor, Tampa, FL 33612, USA; eespana@usf.edu.
Kirill V. Larin, 3517 Cullen Blvd, Room 2027, Houston, TX 77204-5060, USA; klarin@uh.edu.

AN, YSA, and CZD contributed equally to this work.

Received: August 16, 2022
Accepted: October 19, 2022
Published: November 16, 2022

Citation: Nair A, Ambekar YS, Zevallos-Delgado C, et al. Multiple optical elastography techniques reveal the regulation of corneal stiffness by collagen XII. *Invest Ophthalmol Vis Sci.* 2022;63(12):24. https://doi.org/10.1167/iovs.63.12.24

Purpose. Collagen XII plays a role in regulating the structure and mechanical properties of the cornea. In this work, several optical elastography techniques were used to investigate the effect of collagen XII deficiency on the stiffness of the murine cornea.

Methods. A three-prong optical elastography approach was used to investigate the mechanical properties of the cornea. Brillouin microscopy, air-coupled ultrasonic optical coherence elastography (OCE) and heartbeat OCE were used to assess the mechanical properties of wild type (WT) and collagen XII–deficient (*Col12a1*$^{-/-}$) murine corneas. The Brillouin frequency shift, elastic wave speed, and compressive strain were all measured as a function of intraocular pressure (IOP).

Results. All three optical elastography modalities measured a significantly decreased stiffness in the *Col12a1*$^{-/-}$ compared to the WT ($P < 0.01$ for all three modalities). The optical coherence elastography techniques showed that mean stiffness increased as a function of IOP; however, Brillouin microscopy showed no discernable trend in Brillouin frequency shift as a function of IOP.

Conclusions. Our approach suggests that the absence of collagen XII significantly softens the cornea. Although both optical coherence elastography techniques showed an expected increase in corneal stiffness as a function of IOP, Brillouin microscopy did not show such a relationship, suggesting that the Brillouin longitudinal modulus may not be affected by changes in IOP. Future work will focus on multimodal biomechanical models, evaluating the effects of other collagen types on corneal stiffness, and in vivo measurements.

Keywords: optical coherence elastography, biomechanics, Brillouin microscopy, collagen XII

The mechanical properties of the cornea are important for understanding its structure, function, and contribution to overall ocular health.[1,2] Various ocular pathologies and treatments alter these properties, such as keratoconus[3] and corneal collagen cross-linking.[4] Although several tools and technologies have been developed to investigate the mechanical properties of the cornea, applications have been primarily geared toward diagnostics and treatment monitoring, and some clinical devices have made significant contributions toward that goal.[5,6] However, analyzing the biomechanical effects of specific components of the cornea that are critical to its structural integrity is an area that needs further investigation. In particular, the organization and structure of the corneal stroma are of particular relevance as it makes up 90% of the cornea.[7] The relationship between collagen fibril orientation in the stroma and its stiffness has been studied,[8–10] and there have also been focused studies evaluating how the absence of particular collagen proteins affect corneal stiffness.[11] In this study, we investigate the effect of collagen XII[12] on the stiffness of the corneal stroma.

The specific function of collagen XII in the cornea is not well understood, but it is upregulated during stromal wound healing and is present in stromal scars.[13] Furthermore, the literature suggests that this protein is critical for

the development of the cornea,[14,15] regulates tissue structure and function,[16,17] and cell organization[16] and its expression is influenced by mechanical forces.[18] As such, understanding the effects that collagen XII has on the biomechanical properties of the cornea would uncover the effects of this protein on corneal biomechanical properties, structure, and function. Elastography techniques would be particularly well-suited to assess the biomechanical properties of the cornea.[19,20] Ultrasound elastography[21] has been utilized to assess the mechanical properties of the cornea effectively.[22] As with many diseases,[23] studies that examine the effects of individual corneal components are often performed in a murine model. Despite recent advances in this technology to improve resolution and displacement sensitivity,[24] ultrasound elastography is still ill-suited to perform measurements in the small and thin tissue structures such as murine ocular tissues. Similar limitations (e.g., resolution) restrict the use of other clinical elastography methods, such as magnetic resonance elastography.[25]

Optical elastography techniques[19] are well suited for measuring the mechanical properties of the murine cornea due to the superior resolution and sensitivity of optical imaging modalities.[5] Optical elastography methods are largely composed of Brillouin microscopy (BM)[26] and optical coherence elastography (OCE).[27] Brillouin microscopy is an imaging modality that measures spectral changes in scattered light in a sample based on spontaneous pressure and density fluctuations within a sample.[28] These fluctuations are related to the viscoelastic properties of a material. Brillouin microscopy is an all-optical modality and has been effectively used to map the depth-wise mechanical properties in ocular tissues, including the cornea, lens, and the retina.[29–32] However, decoupling sample hydration and viscoelasticity from the Brillouin modulus signature is a non-trivial problem in biological tissue, which results into challenges establishing a fundamental relationship between the Brillouin modulus and Young's modulus.[33,34]

Optical coherence elastography (OCE),[35–38] on the other hand, enables the assessment of material mechanical properties by using optical coherence tomography (OCT)[39] to image and detect tissue response to an excitation force. The measured tissue response is then translated to mechanical properties with an appropriate mechanical model. Generally, OCE methods are subdivided based on the temporal properties of the excitation force,[36] either dynamic[37] or static/quasi-static.[38] Dynamic OCE techniques are largely wave based, where the measured tissue response is in the form of the propagation of an elastic wave. This wave can be induced using a variety of methods, including but not limited to a piezoelectric transducer,[40] air puff,[41] or air-coupled ultrasound transducer (ACUS) [42,43] and has been performed regularly to study the mechanical properties of ocular tissues,[5,38] including the cornea.[5] On the other hand, quasistatic methods typically involve detecting sample response to slow rate displacements, such as inter-frame compression by a mechanical actuator or the heartbeat induced ocular pulse,[44,45] which have also been used to study the biomechanical properties of the cornea.[46–48]

In this work, we used BM, air-coupled ultrasonic optical coherence elastography (ACUS-OCE), and heartbeat OCE (Hb-OCE) to assess the mechanical properties of collagen XII deficient (*Col12a1*$^{-/-}$) corneas in comparison to wild type (WT) corneas. Each of these methods provides complementary information regarding the mechanical properties of the tissue. BM provides biomechanical analysis of tissues at high frequency and high resolution independent of corneal boundary conditions. The Lamb wave propagation speed measured by ACUS-OCE can be translated to shear modulus and represents the shear mechanical properties of the cornea.[49] Hb-OCE, although typically semi-quantitative, can effectively measure the compressive mechanical properties of the cornea (i.e., along the axial direction) and can provide quantitative information when the ocular pulse-induced pressure fluctuation is known.[45] Using these optical methods, we investigate how the absence of collagen XII affects corneal stiffness in a murine model.

Methods

Sample Preparation

Fresh, whole eyes from C57BL/6 and 129/SvJ mixed background mice were shipped overnight in corneal preservation media (Optisol; Chiron Ophthalmics, Irvine, CA, USA)[50] and separated into batches for measurement by each optical elastography modality. All experiments were concluded within 48 hours of enucleation. WT and collagen XII deficient (*Col12a1*$^{-/-}$) corneas were dissected from the whole eye globes with a scleral ring intact. Before measurement, the corneoscleral buttons were mounted on a three-dimensional printed artificial anterior chamber with a 2.3 mm opening for liquid infusion and withdrawal. The mount was connected to a closed-loop intraocular pressure (IOP) control system, which consisted of a custom artificial anterior chamber, pressure transducer, and micro-infusion pump.[51] Corneoscleral buttons were pressurized with a solution of 1× phosphate-buffered saline solution. Optical elastography measurements were taken in the range of 10 mmHg to 25 mmHg at 5 mmHg intervals, and pressure was held constant at each interval to allow the internal pressure to settle. Corneal hydration was maintained with regular topical addition of 1× phosphate-buffered saline solution.

Brillouin Microscopy

Brillouin microscopy was performed in WT (n = 5) and *Col12a1*$^{-/-}$ (n = 5) corneas using a home-built setup[52] consisting of a 660 nm single-mode laser source (Torus; Laser Quantum Inc., Fremont, CA, USA), with 35 mW power on the sample. The Brillouin frequency shift was detected by a spectrometer composed of a dual-stage virtually imaged phase array spectrometer[53] with 30 GHz of free spectral range. The Brillouin spectrometer was calibrated with standard materials, including water and acetone before each measurement. Brillouin measurements were acquired with a microscope objective with 0.25 numerical aperture, resulting in an axial resolution of ~36 µm and lateral resolution of ~3.8 µm, measured using a beam profiler (LaserCam-HR II; Coherent Inc., Santa Clara, CA, USA). The backscattered light collected from the sample was transferred to the dual-stage virtually imaged phase array spectrometer through a single-mode optical fiber. An electron multiplying charge coupled device camera (iXon Andor, Belfast, United Kingdom) was used to detect the Brillouin frequency shift. The exposure time of the camera was 0.1 second during all the measurements. Brillouin images were acquired along a 1.5 mm lateral region at the apex of the cornea (50 pixels) and 120 µm axially (25 axial pixels along the thickness of the cornea). The total acquisition period was 125 seconds per sample. As shown in Fig. 1a), the Brillouin system was co-aligned

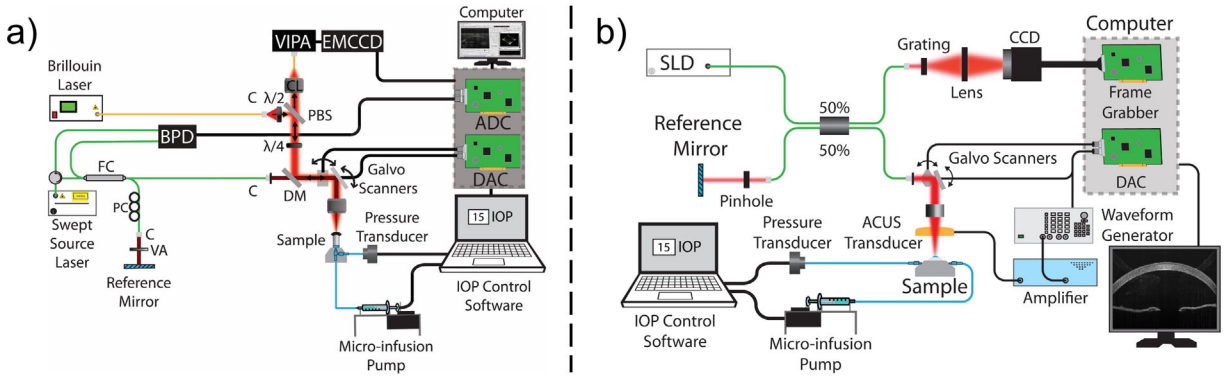

Figure 1. (a) Brillouin/OCT microscopy system schematic. (b) OCE system schematic. ADC, analog to digital converter; BPD, balanced photodetector; C, collimator; CCD, charged coupled device; DAC, digital to analog converter; DM, dichroic mirror; EMCCD, electron multiplying CCD; FC, fiber coupler; PBS, polarizing beam splitter; PC, polarization controller; SLD, superluminescent diode; VA, variable attenuator; VIPA, virtually imaged phase array; λ/4, quarter wave plate.

with a swept-source OCT system with a central wavelength of 1310 nm, bandwidth of 105 nm, and A-scan rate of 50 kHz for image-guided Brillouin measurements.[52]

ACUS-OCE

ACUS-OCE[43] measurements were performed in WT (n = 4) and *Col12a1*$^{-/-}$ (n = 4) corneas with an 840 ± 25 nm wavelength SD-OCT system, with ~6 µm axial resolution, ~8 µm transverse resolution, and ~0.5 nm displacement stability. A spherically focused ACUS transducer with a ~34 mm diameter and ~10 mm diameter round opening was co-focused with the OCT sample beam.[43] The transducer had a central resonance frequency of 1 MHz and was mounted ~20 mm away from the surface of the tissue, equivalent to its focal length. Excitation was performed using three cycles of a 3 kHz square pulse (50% duty cycle) amplitude modulating a continuous 1 MHz signal. The pressure exerted by the transducer at this excitation frequency was measured as 40.78 ± 7.57 kPa by needle hydrophone, and 99% of this pressure is reflected to induce a displacement in the tissue.[54] This signal was then amplified using a radio-frequency amplifier (A150; Electronics & Innovation, Rochester, NY, USA) before driving the ACUS transducer.

OCE measurements were taken in M-B-mode configuration[36] at 50 kHz A-line scan rate with M-scan length of 1000 A-lines acquired along time (20 ms) at each imaging position. The ACUS-induced displacement produced at the corneal apex resulted in the propagation of a Lamb wave across the cornea. The wave propagation was sampled over 251 positions along the lateral direction over a 3.8 mm region across the center of the cornea. Each measurement took approximately five seconds. Peak tracking was used to calculate the time it took for the wave to propagate across the tissue and thereby estimate the elastic wave speed.

Hb-OCE

Hb-OCE[45] measurements were performed in WT (n = 4), and *Col12a1*$^{-/-}$ (n = 5) corneas using the same SD-OCT system. The ocular pulse was simulated using an induced sinusoidal fluctuation of IOP with a 2 mm Hg peak to peak amplitude and 5 s period using the closed loop IOP system for each baseline IOP (10 mm Hg to 25 mm Hg with 5 mm Hg increments). Images with a B-scan size of 1000 A-lines were acquired across a central 3 mm region of the cornea over three IOP cycles, or 15 seconds. The IOP was synchronously recorded with the OCE imaging, and the IOP was co-registered with the OCE images. Axial motion between successive images was detected using a complex conjugate method, and the inter-frame phase difference depicting the corneal motion was denoised using a vector averaging technique[55] using a 15 µm isometric kernel. This phase motion was translated to displacement, which was then normalized to the surface of the cornea such that the inter-frame motion at the corneal surface was 0 for each A-line for each frame. A least squares linear regression algorithm was used to translate the axial displacement measured at each A-line to strain using a 30 µm axial kernel.[56] The average strain for each frame over time was calculated for the 15 second measurement period. The average peak strain over multiple cycles was reported as the strain of each sample at each baseline IOP. A more detailed description of the Hb-OCE technique is described in previous work.[45] Because the amplitude of the IOP, or the stress on the cornea, was recorded between samples, this strain value corresponds to the stiffness of the cornea. It should be noted that a high strain corresponds to a lower stiffness, and a low strain corresponds to a higher stiffness.

The schematic for the OCE system that was used to acquire ACUS-OCE and Hb-OCE measurements is shown in Fig. 1b).

Results

OCT intensity images for representative samples of the WT and *Col12a1*$^{-/-}$ corneas are shown in Figures 2a and 2b, respectively. Corneas are shown mounted on the IOP control system at 20 mm Hg. Note that there is a distinct visual difference between the corneas.

The results of Brillouin microscopy are shown in Figure 3. Figures 3a and 3b show representative Brillouin microscopy images of a WT and *Col12a1*$^{-/-}$ sample, respectively. Figure 3c shows the Brillouin frequency shift distribution at each IOP as a box and whisker plot, where the box corresponds to the interquartile range, the whiskers are 1.5 times the interquartile range, the line through the middle of the box corresponds to the median, and the hollow central box corresponds to the mean. Although Brillouin microscopy does not show a distinct relationship between

Investigative Ophthalmology & Visual Science

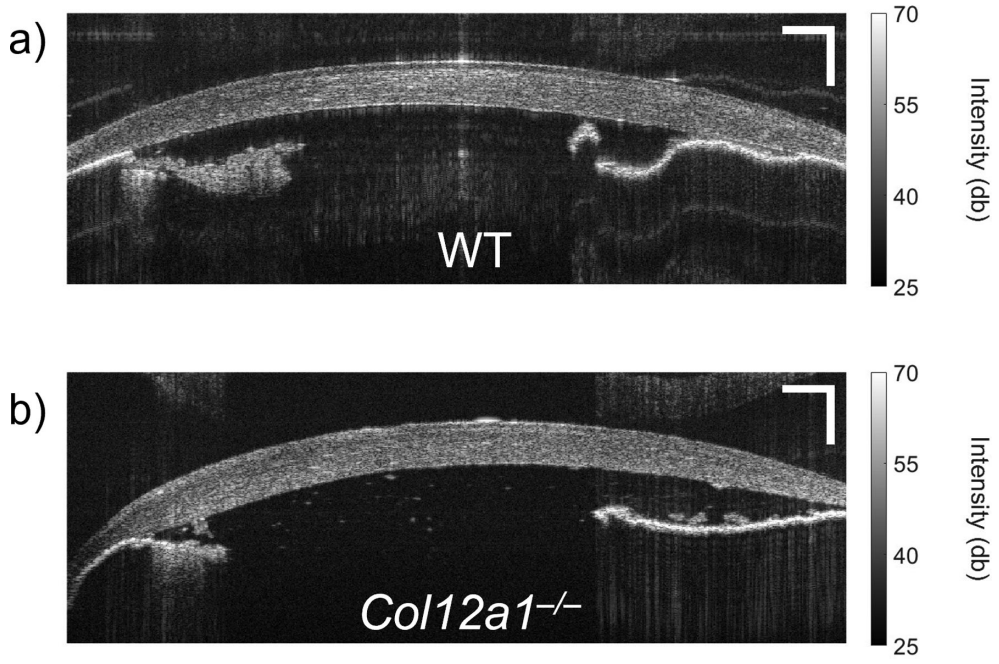

Figure 2. OCT intensity image of a representative (a) WT and (b) *Col12a1*$^{-/-}$ murine cornea. *Scale bars:* 250 µm.

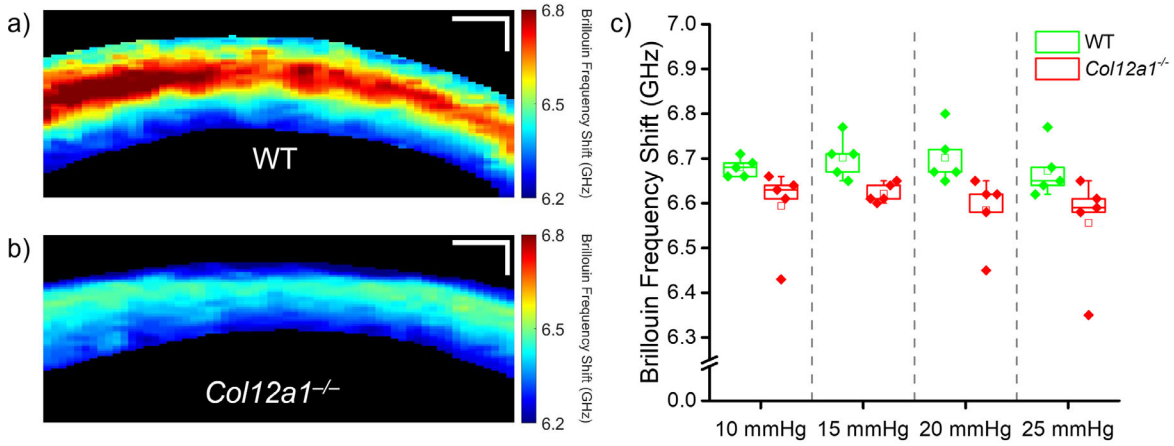

Figure 3. Brillouin microscopy images of a representative (a) WT and (b) *Col12a1*$^{-/-}$ cornea at 10 mm Hg IOP. (c) Box and whisker plot of the Brillouin frequency shift for all measured samples (WT: N=5, and *Col12a1*$^{-/-}$: N = 5), where the *box* represents the interquartile range (IQR), and the *whiskers* represent 1.5 times the IQR. Each points represents the mean sample Brillouin frequency shift. *Scale bars:* 100 µm.

the Brillouin shift and IOP, there was a statistically significant difference (Mann-Whitney U-test, U = 378.5, $P < 0.001$) between the Brillouin frequency shift in WT and the *Col12a1*$^{-/-}$ corneas. On average, the Brillouin shift in the WT corneas was approximately 1.5% higher than the *Col12a1*$^{-/-}$ corneas, which corresponds to an approximately 3% difference in Brillouin modulus, calculated using the methods described in previous work.[57]

The results of the ACUS-OCE measurements are shown below in Figure 4. Figures 4a and 4b show the ACUS-OCE wave speed maps for representative WT and *Col12a1*$^{-/-}$ samples, respectively. Figure 4c shows the sample distribution in box and whisker plots as previously explained. The results show an expected increase in Lamb wave speed as a function of IOP in both groups of corneas. Furthermore, the difference in wave speed in corneas of both tissue types was statistically significant by a Mann Whitney U-test (U = 229, $p < 0.001$), where the average wave speed in the WT corneas was 36% higher.

Finally, the results of the Hb-OCE measurements are shown in Figure 5. Figures 5a and 5b show the Hb-OCE elastograms for representative WT and *Col12a1*$^{-/-}$ corneas, respectively, and Figure 5c shows the distribution of the average strain measured from each sample. To maintain consistency with previous work in Hb-OCE, compressive strain is shown as a positive value. The elastograms shown

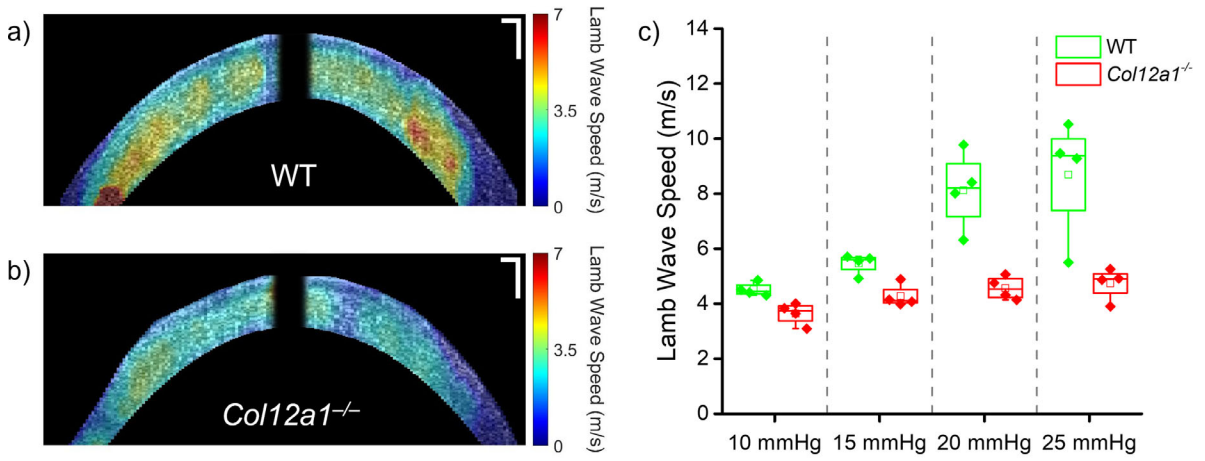

Figure 4. ACUS-OCE wave speed maps of a representative (a) WT and the (b) *Col12a1*$^{-/-}$ cornea at 10 mm Hg IOP. (c) Box and whisker plot of the Lamb wave speed for all measured samples (n = 4 WT and n = 4 *Col12a1*$^{-/-}$), where the *box* represents the interquartile range (IQR), and the *whiskers* represent 1.5 times the IQR. Each point represents the mean sample Lamb wave speed. *Scale bars:* 100 µm.

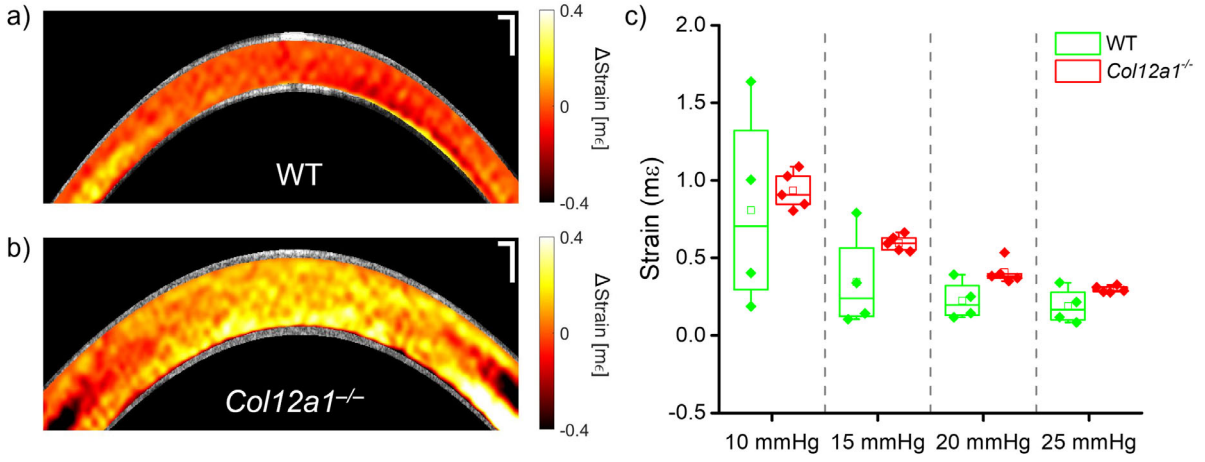

Figure 5. Hb-OCE elastograms of a representative (a) WT and the (b) *Col12a1*$^{-/-}$ cornea at 10 mm Hg IOP. (c) Box and whisker plot of the compressive strain for all measured samples (n = 4 WT and n = 5 *Col12a1*$^{-/-}$), where the *box* represents the interquartile range (IQR), and the *whiskers* represent 1.5 times the IQR. Each points represents the mean sample strain. *Scale bars:* 100 µm.

here illustrate the instantaneous strain at peak IOP elevation rate when the IOP-induced displacement is at its highest. Details regarding the Hb-OCE elastograms are beyond the scope of this work but have been detailed in previous publications.[45,46] Note that in these measurements, the amplitude of the sinusoidal IOP fluctuation was kept similar for all samples, meaning that the measured strain is comparable between samples. Strain measured by Hb-OCE is inversely related to Young's modulus in the axial direction, such that a low strain indicates high stiffness. Note that whereas mean strain decreases (i.e., stiffness increases) as a function of IOP in both the WT and the *Col12a1*$^{-/-}$ corneas, the mean strain in the *Col12a1*$^{-/-}$ corneas was greater than in the WT corneas. Overall, the strain in the *Col12a1*$^{-/-}$ corneas was 44% greater than in the WT corneas. A Mann-Whitney U-test comparing the mean strains of both sample types showed a statistically significant difference between both groups ($U = 80$, $P < 0.01$) at the 0.05 significance level. Furthermore, there was a nonlinear decrease in the strain as a function of IOP in both sample types.

Finally, the Table summarizes the data shown in Figures 3 to 5. An analysis of variance test performed on each tissue group showed an insignificant difference in Brillouin frequency shift as a function of IOP ($df = 3$, $F = 0.49$, $P = 0.70$). An statistically insignificant relationship ($df = 3$, $F = 2.36$, $P = 0.12$) between measured compressive strains at different IOPs was also detected in the WT corneas measured by Hb-OCE, presumably because of the large variance in strain measured within that group, although the mean strain does decrease as a function of IOP. However, there was a statistically significant difference in wave speed as a function of IOP measured by ACUS-OCE in both the WT ($df = 3$, $F = 9.3$, $P = 0.002$) and *Col12a1*$^{-/-}$ ($df = 3$, $F = 4.4$, $P = 0.03$) corneas, and a statistically significant difference in stiffness as a function of IOP in the *Col12a1*$^{-/-}$ corneas measured by Hb-OCE ($df = 3$, $F = 67.9$, $P < 0.001$).

Table. Summary of Optical Elastography Results for WT and *Col12a1*$^{-/-}$ Corneas for Each Measured IOP

	Brillouin Frequency Shift (GHz)		Lamb Wave Speed (m/s)		Compressive Strain (mε)	
	WT	*Col12a1*$^{-/-}$	WT	*Col12a1*$^{-/-}$	WT	*Col12a1*$^{-/-}$
10 mm Hg	6.68 ± 0.02	6.59 ± 0.9	4.52 ± 0.24*	3.64 ± 0.39*	0.81 ± 0.65	0.93 ± 0.12*
15 mm Hg	6.70 ± 0.04	6.62 ± 0.02	5.46 ± 0.37*	4.27 ± 0.41*	0.34 ± 0.31	0.60 ± 0.05*
20 mm Hg	6.70 ± 0.06	6.59 ± 0.07	8.13 ± 1.42*	4.57 ± 0.42*	0.23 ± 0.12	0.42 ± 0.08*
25 mm Hg	6.68 ± 0.05	6.56 ± 0.01	8.69 ± 2.20*	4.9 ± 0.58*	0.19 ± 0.11	0.30 ± 0.02*

* Statistical significance as a function of IOP tested by analysis of variance ($P < 0.05$).

Discussion

In this work, we examine how collagen XII regulates the mechanical properties of the cornea. Our results suggest that collagen XII regulates corneal stroma stiffness based on multiple metrics. Measurements were performed ex vivo at various artificially controlled IOPs. ACUS-OCE and Hb-OCE both illustrate that collagen XII deficiency resulted in decreased corneal stiffness compared to WT corneas, and that corneal stiffness increased as a function of IOP regardless of collagen XII presence. Brillouin microscopy results showed the same trend where collagen XII deficient corneas had lower longitudinal modulus compared to the WT corneas. However, the measured Brillouin frequency shift had no apparent dependence on the IOP in either condition. IOP is known to affect the stiffness of the cornea and does affect corneal elastography measurements. In practice, though, IOP is known to confound measurements in clinical tools for biomechanical assessment.[6] Thus the result from this work suggests that the Brillouin frequency shift may, in fact, provide a mechanical measurement that is independent of the effects of IOP. At a fundamental level, it remains to be investigated why the longitudinal modulus measured by Brillouin microscopy seems unaffected by changes in IOP unlike the OCE measurements, and how the current sensitivity of the measurement, or the measurement conditions (e.g., orthogonal to the collagen fiber direction)[58] contribute to these results. In addition, corneal stiffness is known to be affected by age and sex.[59] In this study, the age and sex of the corneas were not strictly controlled, which likely did introduce some variation in the results, particularly in the WT group. Furthermore, the same cornea was not measured between each technique, which may also have introduced some sample variability in the results. Moreover, collagen XII contribution to the corneal structure is age-dependent.[60] Future work will conduct more strict sex and age matching, which will help tighten variation in corneal stiffness.

OCE has also been used to study the effects of collagen V insufficiency on corneal stiffness.[11] Collagen V insufficiency was reported to have increased stiffness compared to the WT, and this measurement was confirmed by two-dimensional extensiometry. The results of our work suggest that collagen XII may have opposing influences on the mechanical properties of the cornea. It should also be noted that the results of our work contradict previous atomic force microscopy (AFM) measurements of collagen XII deficient corneas.[60] However, in that study, the AFM indentation was kept at approximately 1 µm, well within the cornea epithelium thickness. Since the effect of collagen XII deficiency is likely localized to the corneal stroma, measurements of the corneal epithelium may not accurately characterize changes in stromal stiffness. That suggests that the reduced fibrillar diameter and increased fibrillar density of the cornea in the absence of collagen XII identified in that work may actually contribute to the reduced stiffness of the collagen XII deficient cornea compared to the WT in this work.

Although each individual measurement technique of our elastography approach shows agreement regarding the difference in stiffness between the two measurement groups, these measurements are not without limitations. Primarily, although each of these techniques can be useful for estimating changes in stiffness, we have not quantified the elastic modulus. The high-frequency longitudinal modulus can be extracted from the Brillouin shift measurement. However, the longitudinal modulus is a fundamentally different quantity than Young's modulus, and the correlations between these moduli measured in biological tissue are thought to come from a common dependence from underlying factors such as collagen branching, crosslinking, and water content. In this respect, our work hints that IOP dependence represents a situation where the two moduli exhibit different behavior. Relating the Brillouin modulus to Young's modulus measured by OCE and viscosity[61,62] is an area of future investigation. Furthermore, although the ex vivo studies performed in this work provide valuable information, translating Brillouin microscopy measurements to in vivo assessment of corneal stiffness introduces measurement tradeoffs in terms of the number of samples acquired in measurement to prevent the effects of motion artifacts and to reduce subject discomfort. However, OCT guidance[52] could be used to correct the motion. Brillouin microscopy has been performed in vivo in murine embryos[52] and humans.[30,52]

The Lamb wave propagation and analysis technique utilized by ACUS-OCE can provide quantitative measurements of elasticity and can be performed in vivo.[43,63] However, proper analysis of mechanical properties could be improved by analyzing elastic wave dispersion (i.e., multiple frequencies) and taking into consideration the sample geometry. This analysis would enable the assessment of corneal Young's modulus and shear viscosity. It should be noted that the distinct differences in corneal geometry between the WT and *Col12a1*$^{-/-}$ corneas could affect the stiffness measurements by ACUS-OCE. In fact, previous work has reported increased thickness in *Col12a1*$^{-/-}$ corneas.[64] Typically, a thicker material with the same stiffness has a higher wave speed up to a certain limit. Because the *Col12a1*$^{-/-}$ corneas had a lower wave speed compared to their WT counterparts, we can conclude that the *Col12a1*$^{-/-}$ are indeed softer than the WT. However, applying mathematical models that account for corneal geometry, including the differences in thickness, to quantitatively derive mechanical properties

Investigative Ophthalmology & Visual Science

such as Young's modulus and viscosity is an area of future work.[65,66]

Finally, Hb-OCE enables axial assessment of strain based on ocular pulse induced IOP fluctuations and has been performed in vivo.[46] However, axial assessment of corneal strain using Hb-OCE is confounded by the visible sample thickness in the OCT image and the size of the strain calculation kernel. The use of a high-resolution OCT system would help dramatically improve Hb-OCE sensitivity. Spatially mapping Young's modulus is a more complex problem, as spatial characterization of stress inside the cornea is necessary for accurate quantification. The average IOP change can be measured in ex vivo measurements, but performing this assessment in vivo would require additional measurements, such as dynamic contour tonometry[67] or the use of a compliant sensor.[68] However, the stress on this cornea was relatively well controlled in this work, because the mean IOP fluctuation amplitude for the WT corneas was 2.04 ± 0.02 mm Hg and was 2.06 ± 0.08 mm Hg for *Col12a1*$^{-/-}$ corneas. Because the difference in IOP fluctuation amplitude between the two types of corneas was negligible, we can assume that the measured and mapped strain represents a more quantitative characterization of corneal stiffness than cases where the stress is far more variable. Furthermore, we demonstrate here for the first time Hb-OCE as a function of baseline IOP and demonstrate the nonlinear relationship between strain and IOP as measured by this technique. Because the strain and stiffness are inversely related, the nonlinear strain-IOP relationship shown here may correlate to a more linear stiffness-IOP relationship when elasticity is properly accounted for (i.e., 1/strain is linear as a function of IOP). The results shown here emphasize the need for more robust quantification of elasticity for future Hb-OCE measurements.[11,69]

Conclusion

In this work, a multiple optical elastography approaches consisting of Brillouin microscopy, ACUS-OCE, and Hb-OCE were used to assess the effects of collagen XII deficiency on the mechanical properties of the cornea. *Col12a1*$^{-/-}$ and WT murine cornea samples were excised so that the scleral ring was left intact, then mounted on a closed-loop IOP control system. Elastography measurements were performed at IOPs between 10 mm Hg and 25 mm Hg at 5 mm Hg increments. OCE measured a change in stiffness as a function of IOP, but Brillouin microscopy showed no clear trend between IOP and the Brillouin frequency shift. Furthermore, the results suggest that collagen XII deficiency reduces the overall stiffness of the cornea. Future work will investigate the effects of other collagen types and cornea components (e.g., glycosaminoglycans) on the stiffness of the cornea, implement appropriate mechanical models, and translate this work in vivo.

Acknowledgments

Supported by the National Institutes of Health, grant numbers R01EY022362, R01EY030063, R01EY029395, R01EY028666, and P30EY007551.

Disclosure: **A. Nair**, None; **Y.S. Ambekar**, None; **C. Zevallos-Delgado**, None; **T. Mekonnen**, None; **M. Sun**, None; **F. Zvietcovich**, None; **M. Singh**, None; **S. Aglyamov**, None; **M. Koch**, None; **G. Scarcelli**, None; **E.M. Espana**, None; **K.V. Larin**, None

References

1. Kling S, Hafezi F. Corneal biomechanics—a review. *Ophthalmic Physiol Opt*. 2017;37:240–252.
2. Ma J, Wang Y, Wei P, Jhanji V. Biomechanics and structure of the cornea: implications and association with corneal disorders. *Surv Ophthalmol*. 2018;63:851–861.
3. Bao F, Geraghty B, Wang Q, Elsheikh A. Consideration of corneal biomechanics in the diagnosis and management of keratoconus: is it important? *Eye Vis (Lond)*. 2016;3:18.
4. Meek KM, Hayes S. Corneal cross-linking—a review. *Ophthalmic Physiol Opt*. 2013;33:78–93.
5. Kirby MA, Pelivanov I, Song S, et al. Optical coherence elastography in ophthalmology. *J Biomed Opt*. 2017;22:1–28.
6. Pinero DP, Alcon N. Corneal biomechanics: a review. *Clin Exp Optom*. 2015;98:107–116.
7. Maurice DM. The structure and transparency of the cornea. *J Physiol*. 1957;136:263–286.
8. Leonard BC, Cosert K, Winkler M, et al. Stromal collagen arrangement correlates with stiffness of the canine cornea. *Bioengineering (Basel)*. 2019;7:4.
9. Winkler M, Shoa G, Xie Y, et al. Three-dimensional distribution of transverse collagen fibers in the anterior human corneal stroma. *Invest Ophthalmol Vis Sci*. 2013;54:7293–7301.
10. Daxer A, Fratzl P. Collagen fibril orientation in the human corneal stroma and its implication in keratoconus. *Invest Ophthalmol Vis Sci*. 1997;38:121–129.
11. Kling S, Torres-Netto EA, Abdshahzadeh H, Espana EM, Hafezi F. Collagen V insufficiency in a mouse model for Ehlers Danlos-syndrome affects viscoelastic biomechanical properties explaining thin and brittle corneas. *Sci Rep*. 2021;11:17362.
12. Gordon MK, Gerecke DR, Dublet B, van der Rest M, Sugrue SP, Olsen BR. The structure of type XII collagen. *Ann N Y Acad Sci*. 1990;580:8–16.
13. Massoudi D, Malecaze F, Soler V, et al. NC1 long and NC3 short splice variants of type XII collagen are overexpressed during corneal scarring. *Invest Ophthalmol Vis Sci*. 2012;53:7246–7256.
14. Young BB, Zhang G, Koch M, Birk DE. The roles of types XII and XIV collagen in fibrillogenesis and matrix assembly in the developing cornea. *J Cell Biochem*. 2002;87:208–220.
15. Gordon MK, Foley JW, Lisenmayer TF, Fitch JM. Temporal expression of types XII and XIV collagen mRNA and protein during avian corneal development. *Dev Dyn*. 1996;206:49–58.
16. Marchant JK, Zhang G, Birk DE. Association of type XII collagen with regions of increased stability and keratocyte density in the cornea. *Exp Eye Res*. 2002;75:683–694.
17. Sun M, Koudouna E, Cogswell D, Avila MY, Koch M, Espana EM. Collagen XII regulates corneal stromal structure by modulating transforming growth factor-beta activity. *Am J Pathol*. 2022;192:308–319.
18. Arai K, Nagashima Y, Takemoto T, Nishiyama T. Mechanical strain increases expression of type XII collagen in murine osteoblastic MC3T3-E1 cells. *Cell Struct Funct*. 2008;33:203–210.
19. Kennedy BF, Wijesinghe P, Sampson DD. The emergence of optical elastography in biomedicine. *Nat Photonics*. 2017;11:215–221.
20. Li Y, Snedeker JG. Elastography: modality-specific approaches, clinical applications, and research horizons. *Skeletal Radiol*. 2011;40:389–397.
21. Ophir J, Cespedes I, Ponnekanti H, Yazdi Y, Li X. Elastography: a quantitative method for imaging the elasticity of biological tissues. *Ultrason Imaging*. 1991;13:111–134.

22. Qian X, Ma T, Shih CC, et al. Ultrasonic microelastography to assess biomechanical properties of the cornea. *IEEE Trans Biomed Eng*. 2019;66:647–655.
23. Bedell MA, Jenkins NA, Copeland NG. Mouse models of human disease. Part I: techniques and resources for genetic analysis in mice. *Genes Dev*. 1997;11:1–10.
24. Clayson K, Pavlatos E, Pan X, Sandwisch T, Ma Y, Liu J. Ocular pulse elastography: imaging corneal biomechanical responses to simulated ocular pulse using ultrasound. *Transl Vis Sci Technol*. 2020;9:5.
25. Muthupillai R, Lomas DJ, Rossman PJ, Greenleaf JF, Manduca A, Ehman RL. Magnetic resonance elastography by direct visualization of propagating acoustic strain waves. *Science*. 1995;269:1854–1857.
26. Prevedel R, Diz-Muñoz A, Ruocco G, Antonacci G. Brillouin microscopy: an emerging tool for mechanobiology. *Nat Methods*. 2019;16:969–977.
27. Schmitt J. OCT elastography: imaging microscopic deformation and strain of tissue. *Opt Express*. 1998;3:199–211.
28. Scarcelli G, Yun SH. Confocal Brillouin microscopy for three-dimensional mechanical imaging. *Nat Photonics*. 2007;2:39–43.
29. Scarcelli G, Pineda R, Yun SH. Brillouin optical microscopy for corneal biomechanics. *Invest Ophthalmol Vis Sci*. 2012;53:185–190.
30. Scarcelli G, Yun SH. In vivo Brillouin optical microscopy of the human eye. *Opt Express*. 2012;20:9197–9202.
31. Ambekar YS, Singh M, Zhang J, et al. Multimodal quantitative optical elastography of the crystalline lens with optical coherence elastography and Brillouin microscopy. *Biomed Opt Express*. 2020;11:2041–2051.
32. Ambekar YS, Singh M, Scarcelli G, et al. Characterization of retinal biomechanical properties using Brillouin microscopy. *J Biomed Opt*. 2020;25(9):090502.
33. Wu PJ, Kabakova IV, Ruberti JW, et al. Water content, not stiffness, dominates Brillouin spectroscopy measurements in hydrated materials. *Nat Methods*. 2018;15:561–562.
34. Scarcelli G, Yun SH. Reply to "Water content, not stiffness, dominates Brillouin spectroscopy measurements in hydrated materials." *Nat Methods*. 2018;15:562–563.
35. Larin KV, Sampson DD. Optical coherence elastography—OCT at work in tissue biomechanics [Invited]. *Biomed Opt Express* .2017;8:1172–1202.
36. Singh M, Zvietcovich F, Larin KV. Introduction to optical coherence elastography: tutorial. *J Opt Soc Am A Opt Image Sci Vis*. 2022;39:418–430.
37. Zaitsev VY, Matveyev AL, Matveev LA, et al. Strain and elasticity imaging in compression optical coherence elastography: the two-decade perspective and recent advances. *J Biophotonics*. 2021;14:e202000257.
38. Zvietcovich F, Larin KV. Wave-based optical coherence elastography: the 10-year perspective. *Prog Biomed Eng (Bristol)*. 2022;4:012007.
39. Huang D, Swanson EA, Lin CP, et al. Optical coherence tomography. *Science*. 1991;254:1178–1181.
40. Ramier A, Tavakol B, Yun SH. Measuring mechanical wave speed, dispersion, and viscoelastic modulus of the cornea using optical coherence elastography. *Opt Express*. 2019;27:16635–16649.
41. Wang S, Larin KV, Li J, et al. A focused air-pulse system for optical-coherence-tomography-based measurements of tissue elasticity. *Laser Phys Lett*. 2013;10:075605.
42. Ambrozinski L, Song S, Yoon SJ, et al. Acoustic microtapping for non-contact 4D imaging of tissue elasticity. *Sci Rep*. 2016;6:38967.
43. Zvietcovich F, Nair A, Ambekar YS, et al. Confocal air-coupled ultrasonic optical coherence elastography probe for quantitative biomechanics. *Opt Lett*. 2020;45:6567–6570.
44. Kennedy BF, McLaughlin RA, Kennedy KM, et al. Optical coherence micro-elastography: mechanical-contrast imaging of tissue microstructure. *Biomed Opt Express*. 2014;5:2113–2124.
45. Nair A, Singh M, Aglyamov SR, Larin KV. Heartbeat OCE: corneal biomechanical response to simulated heartbeat pulsation measured by optical coherence elastography. *J Biomed Opt*. 2020;25:1–9.
46. Nair A, Singh M, Aglyamov S, Larin KV. Heartbeat optical coherence elastography: corneal biomechanics in vivo. *J Biomed Opt*. 2021;26:020502.
47. Singh M, Nair A, Aglyamov SR, Larin KV. Compressional optical coherence elastography of the cornea. *Photonics*. 2021;8:111.
48. Ford MR, Dupps WJ, Rollins AM, Sinha RA, Hu Z. Method for optical coherence elastography of the cornea. *J Biomed Opt*. 2011;16:016005.
49. Han Z, Li J, Singh M, et al. Optical coherence elastography assessment of corneal viscoelasticity with a modified Rayleigh-Lamb wave model. *J Mech Behav Biomed Mater*. 2017;66:87–94.
50. Kaufman HE, Beuerman RW, Steinemann TL, Thompson HW, Varnell ED. Optisol corneal storage medium. *Arch Ophthalmol*. 1991;109:864–868.
51. Twa MD, Li J, Vantipalli S, et al. Spatial characterization of corneal biomechanical properties with optical coherence elastography after UV cross-linking. *Biomed Opt Express*. 2014;5:1419–1427.
52. Ambekar YS, Singh M, Schill AW, et al. Multimodal imaging system combining optical coherence tomography and Brillouin microscopy for neural tube imaging. *Opt Lett*. 2022;47:1347–1350.
53. Scarcelli G, Yun SH. Multistage VIPA etalons for high-extinction parallel Brillouin spectroscopy. *Opt Express*. 2011;19:10913–10922.
54. Zvietcovich F, Nair A, Ambekar YS, et al. Confocal air-coupled ultrasonic optical coherence elastography probe for quantitative biomechanics. *Opt Lett*. 2020;45:6567–6570.
55. Matveyev AL, Matveev LA, Sovetsky AA, Gelikonov GV, Moiseev AA, Zaitsev VY. Vector method for strain estimation in phase-sensitive optical coherence elastography. *Laser Phys Lett*. 2018;15:065603.
56. Kennedy BF, Koh SH, McLaughlin RA, Kennedy KM, Munro PR, Sampson DD. Strain estimation in phase-sensitive optical coherence elastography. *Biomed Opt Express*. 2012;3:1865–1879.
57. Ambekar YS, Singh M, Zhang J, et al. Multimodal quantitative optical elastography of the crystalline lens with optical coherence elastography and Brillouin microscopy. *Biomed Opt Express*. 2020;11:2041–2051.
58. Eltony AM, Shao P, Yun S-H. Measuring mechanical anisotropy of the cornea with Brillouin microscopy. *Nat Commun*. 2022;13:1–11.
59. Zhang B, Shweikh Y, Khawaja AP, Gallacher J, Bauermeister S, Foster PJ. Associations with corneal hysteresis in a population cohort: results from 96 010 UK biobank participants. *Ophthalmology*. 2019;126:1500–1510.
60. Sun M, Zafrullah N, Devaux F, et al. Collagen XII Is a Regulator of Corneal Stroma Structure and Function. *Invest Ophthalmol Vis Sci*. 2020;61:61.
61. Margueritat J, Virgone-Carlotta A, Monnier S, et al. High-frequency mechanical properties of tumors measured by Brillouin light scattering. *Phys Rev Lett*. 2019;122:018101.
62. Xu J, Ren X, Gong W, Dai R, Liu D. Measurement of the bulk viscosity of liquid by Brillouin scattering. *Appl Opt*. 2003;42:6704–6709.
63. Zvietcovich F, Nair A, Singh M, Aglyamov S, Twa M, Larin K. In vivo assessment of corneal biomechanics under localized

Investigative Ophthalmology & Visual Science

cross-linking treatment using confocal air-coupled optical coherence elastography. *Biomed Opt Express*. 2022;13:2644–2654.

64. Hemmavanh C, Koch M, Birk DE, Espana EM. Abnormal Corneal Endothelial Maturation in Collagen XII and XIV Null Mice. *Invest Ophthalmol Vis Sci*.2013;54:3297–3308.
65. Han Z, Li J, Singh M, et al. Optical coherence elastography assessment of corneal viscoelasticity with a modified Rayleigh-Lamb wave model. *J Mech Behav Biomed Mater*. 2017;66:87–94.
66. Pitre JJ, Kirby MA, Li DS, et al. Nearly-incompressible transverse isotropy (NITI) of cornea elasticity: model and experiments with acoustic micro-tapping OCE. *Sci Rep*. 2020;10:12983.
67. Kaufmann C, Bachmann LM, Robert YC, Thiel MA. Ocular pulse amplitude in healthy subjects as measured by dynamic contour tonometry. *Arch Ophthalmol*. 2006;124:1104–1108.
68. Kennedy KM, Es'haghian S, Chin L, McLaughlin RA, Sampson DD, Kennedy BF. Optical palpation: optical coherence tomography-based tactile imaging using a compliant sensor. *Opt Lett*. 2014;39:3014–3017.
69. Elsheikh A, Geraghty B, Rama P, Campanelli M, Meek KM. Characterization of age-related variation in corneal biomechanical properties. *J R Soc Interface*. 2010;7:1475–1485.

Investigative Ophthalmology & Visual Science